

A simulation-based analytic model of radio galaxies II: self-consistent radiative losses

M.J. Hardcastle

Centre for Astrophysics Research, Department of Physics, Astronomy and Mathematics, University of Hertfordshire, College Lane, Hatfield AL10 9AB, UK

1 July 2026

ABSTRACT

The evolution of the radio properties of high-redshift radio-luminous active galactic nuclei is well known to be strongly affected by inverse-Compton losses which increase rapidly at higher redshifts due to the higher energy density in the cosmic microwave background radiation. Dynamical models of these sources, however, generally neglect the effects of radiative losses on the dynamics and energetics of the sources themselves. In the framework of an analytical model I developed in a previous paper, I show that the assumption that these losses can be neglected becomes unsafe at high redshifts. The effects on the source dynamics and energetics can result in significantly lower predicted luminosities for high-redshift sources in both radio (synchrotron) and X-ray (inverse-Compton) bands. Modelling of the population of these powerful sources needs to take account of these results in order to infer jet powers at high redshift, and also to make a correct prediction of the number of sources that may be available to provide a background for studies of the 21-cm forest.

Key words: galaxies: jets – galaxies: active – radio continuum: galaxies

1 INTRODUCTION

Observations with current and next-generation radio telescopes increasingly probe the active galaxy population in the distant universe, and evidence for accreting black holes in the very early universe is becoming more and more compelling (e.g. Maiolino et al. 2024). At least some of these accreting black holes might be expected to fulfil the conditions required to generate powerful jets (which are likely to be related to the spin of the black hole and the magnetization of the material in the accretion flow; Blandford & Znajek 1977).

In the local Universe, the effects of these jets are predominantly detected as a result of the radio emission due to synchrotron radiation from high-energy particles accelerated within the jet, but the normalization of this synchrotron emission and its spectrum depends on the details of the acceleration and evolution of the particles within the jets and the large-scale lobes that they inflate. It is therefore important to have a model framework within which we can understand the expected evolution of radio-luminous AGN (RLAGN) at high redshift. In principle this needs to take account of (i) the evolution of the conditions required for jet generation in the first place, (ii) the different local environments experienced by the jets at high redshift, and (iii) the rapid increase in the energy density of the cosmic microwave background radiation, which goes as $(1+z)^4$ and drives inverse-Compton losses (e.g. Wu et al. 2017).

An important application of such a model would be a prediction of the radio properties of the high-redshift radio sources that could be used to give a continuum background against which the so-called ‘21-cm forest’ could be detected (e.g. Mellema et al. 2013). In principle, this absorption signal from the redshifted neutral hydrogen in the Universe along the line of sight to the radio source would give a view of the evolution of neutral hydrogen and particularly the timing

and evolution of the epoch of reionization which is very complementary to studies of neutral hydrogen in emission. The study of high-redshift neutral hydrogen provides one of the key science cases for the forthcoming Square Kilometre Array (Koopmans et al. 2015).

In an earlier paper (Hardcastle 2018, hereafter Paper 1) I described a simulation-based analytic model that is primarily designed to model the evolution of powerful RLAGN, where in this context ‘powerful’ means that the sources have enough kinetic power to drive a shock through their external environment throughout their evolution¹. The key feature of the model was that the energy supplied by the initially light, electron-positron jet is partitioned in a predictable way between the ‘lobes’, containing the synchrotron-emitting particles, and the ‘shocked shell’, consisting of shocked and swept up baryonic matter from the environment. Equally importantly, though, it was assumed that energy was conserved inside the shocked shell: that is, radiative losses from any component of the system were negligible. I showed in Paper 1 that this assumption was reasonable for low-redshift RLAGN, which was the principal use case for the model at the time. However, as I noted in that paper, it seemed likely to break down badly for high-redshift sources where inverse-Compton losses become more and more important. In the present paper I extend the framework of Paper 1 to develop a model in which the losses and the radio source dynamics can be considered consistently, and show that such a model has significant observational consequences at high redshift, affecting the inference

¹ This corresponds roughly to sources above the classical Fanaroff-Riley break (Fanaroff & Riley 1974) which implies jet powers above around 10^{38} W, but of course the ability to drive a shock is also dependent on environment.

of jet powers, the population of high- z luminous radio sources which it is hoped may provide a direct detection of the 21-cm forest, and predictions for future sensitive X-ray surveys.

Throughout the paper I use a standard flat Λ CDM cosmology with $H_0 = 70 \text{ km s}^{-1}$, $\Omega_m = 0.3$ and $\Omega_\Lambda = 0.7$, and define spectral index α in the sense $S \propto \nu^{-\alpha}$.

2 LOSSES

2.1 The problem

Let us start by revisiting some of the assumptions of Paper 1. We describe a RLAGN as having a two-sided jet power Q , and since the jet is initially light and relativistic this implies a jet momentum flux per lobe of $Q/2c$. As noted above, in the absence of losses, all of the jet power goes into the lobes and the shocked shell (the work done on the external environment, in this phase, is all done on the shocked material – by construction, the unshocked medium is unaffected by the AGN). Therefore the total energy in the lobes and shocked shell at any given time t is just Qt . The key simplifying assumption, which is supported by simulations, is that a constant fraction ξ of the energy supplied by the jet is stored in the lobes, while the rest is in the shocked shell. In Paper 1 I went on to derive a dynamical model for the expansion of the lobes through the external medium, which is unchanged in the present paper.

However, it is easy to see that at some point a model like this will lead to an inconsistency. Consider inverse-Compton losses, which for a single electron² of Lorentz factor γ ($\gamma \gg 1$) and a radiation field of energy density U_{rad} can be written (Longair 2010)

$$\frac{dE}{dt} = -\frac{4}{3} \sigma_T c U_{\text{rad}} \gamma^2 \quad (1)$$

where σ_T is the Thomson cross-section and c is the speed of light. For the important case of inverse-Compton scattering from the CMB, we know that $U_{\text{rad}} = 4.2 \times 10^{-14} (1+z)^4 \text{ J m}^{-3}$. The strong dependence on redshift means that the energy density in the CMB, and therefore the loss rate for an electron of a given energy, is 2,400 times higher at $z = 6$ than at $z = 0$.

Suppose that the electron energy distribution in the lobes is given by a power law,

$$N(E) = N_0 E^{-q} \quad (2)$$

where $N(E)$ here is the differential number density of electrons of a particular energy E and N_0 is a normalizing factor. Then we have, assuming as a slight simplification that the energy density in electrons is dominant in the lobes, that

$$\xi Qt = V_{\text{lobe}} \int_{E_{\text{min}}}^{E_{\text{max}}} EN(E) dE = V_{\text{lobe}} N_0 \int_{E_{\text{min}}}^{E_{\text{max}}} E^{1-q} dE = V_{\text{lobe}} N_0 I_E \quad (3)$$

with

$$I_E = \begin{cases} \ln(E_{\text{max}}/E_{\text{min}}) & q = 2 \\ \frac{1}{2-q} \left[E_{\text{max}}^{(2-q)} - E_{\text{min}}^{(2-q)} \right] & q \neq 2 \end{cases} \quad (4)$$

Now the inverse-Compton loss rate for this particle population

² Throughout the paper, except where otherwise stated, I assume that the energy density of the lobes is dominated by a bulk neutral electron/positron plasma; ‘electron’ should be taken to refer to electrons of both charges.

is given by integrating Eq. 1 over the energies of all the available particles:

$$-\frac{dE_{\text{total}}}{dt} = \frac{4}{3} V_{\text{lobe}} \sigma_T c U_{\text{rad}} \int_{E_{\text{min}}}^{E_{\text{max}}} N(E) \left(\frac{E}{m_e c^2} \right)^2 dE \quad (5)$$

giving

$$-\frac{dE_{\text{total}}}{dt} = \frac{4}{3} V_{\text{lobe}} N_0 \frac{\sigma_T U_{\text{rad}}}{m_e^2 c^3} I_{\text{loss}} \quad (6)$$

where similarly

$$I_{\text{loss}} = \begin{cases} \ln(E_{\text{max}}/E_{\text{min}}) & q = 3 \\ \frac{1}{3-q} \left[E_{\text{max}}^{(3-q)} - E_{\text{min}}^{(3-q)} \right] & q \neq 3 \end{cases} \quad (7)$$

The assumption of negligible radiative losses breaks down if the radiative loss becomes comparable to the input jet power, i.e., if $Q \approx |dE/dt|$. Writing down this condition in the case of inverse-Compton losses as an inequality gives

$$Q < \frac{4}{3} V_{\text{lobe}} N_0 \frac{\sigma_T U_{\text{rad}}}{m_e^2 c^3} I_{\text{loss}} \quad (8)$$

for the assumption to break down. But we can use Eq. 3 to eliminate $V_{\text{lobe}} N_0$ from this equation:

$$Q < \frac{4}{3} \frac{\xi Qt}{I_E} \frac{\sigma_T U_{\text{rad}}}{m_e^2 c^3} I_{\text{loss}} \quad (9)$$

Hence these assumptions must have broken down, *independent of Q* , by a time t given by

$$t = \frac{3}{4} \frac{m_e^2 c^3}{\xi \sigma_T U_{\text{rad}}} \frac{I_E}{I_{\text{loss}}} \quad (10)$$

We see that the timescale t on which our approximation breaks down is inversely proportional to the energy density of the CMB, and thus goes as $(1+z)^{-4}$. t is somewhat sensitive to the parameters of the power-law distribution, particularly q and E_{max} , through the ratio I_E/I_{loss} , but adopting $q = 2.1$ (as used in Paper 1) and E_{max} corresponding to $\gamma = 10^4$ (it cannot be less than this if we see radiating electrons at GHz frequencies), and substituting the energy density of the CMB for U_{rad} , we find a critical timescale of over 5 Gyr at $z = 0$, but only around 2 Myr at $z = 6$. Thus, while the effects of inverse-Compton losses can be safely neglected for low-redshift RLAGN, whose lifetimes are likely to be mostly $\ll 1$ Gyr, they absolutely cannot be neglected for objects at high redshift, since Myr timescales are well within the range of lifetimes expected for RLAGN. Indeed, the longest-lived objects should already start to be affected by $z = 1$. Crucially, in this approximation all RLAGN will be affected in the same way independent of their jet power, because to first order inverse-Compton losses scale linearly with the total integrated energy in the lobes, as noted in Paper 1.

Synchrotron losses are more complex because the overall synchrotron loss history depends on the evolving magnetic field strength in the lobes. The loss rate to synchrotron emission is the same as in eq. 1 but with the magnetic field energy density, U_B , being substituted for the radiation energy density. If we assume (as in Paper 1) that the magnetic field total energy is a fixed fraction ζ of the energy in radiating particles, then for $\zeta \ll 1$ we have

$$U_B = \zeta N_0 I_E = \frac{\zeta \xi Qt}{V_{\text{lobe}}} \quad (11)$$

Then our assumptions become invalid when

$$Q < \frac{4}{3} \frac{\xi Qt}{I_E} \frac{\sigma_T}{m_e^2 c^3} \frac{\zeta \xi Qt}{V_{\text{lobe}}} I_{\text{loss}} \quad (12)$$

or, rearranging,

$$\frac{Qt^2}{V_{\text{lobe}}} > \frac{3 m_e^2 c^3}{4 \sigma_T} \frac{1}{\zeta \xi^2} \frac{I_E}{I_{\text{loss}}} \quad (13)$$

where the right-hand side contains only constants of the model. Unlike the inverse-Compton case, this depends on the dynamics through the time-dependent V_{lobe} . In the very early parts of the model of Paper 1, $V_{\text{lobe}} \approx c^3 t^3$, and so the synchrotron loss will always exceed the jet power as $t \rightarrow 0$. This feature of the model can be ignored, as it is only relevant to the time period when the jet has just turned on for the first time, and we can reasonably assume that e.g. particle acceleration or the mechanism to establish local quasi-equipartition of energy do not operate effectively at these times. Otherwise we expect to see any problems only for high Q and at late times if V_{lobe} grows more slowly than t^2 . In practice, this does not occur in even the most extreme modelled jets (Paper 1) and so catastrophic synchrotron losses can safely be neglected.

Finally, I noted in Paper 1 that thermal bremsstrahlung losses from the shocked shell appear likely to be negligible in comparison to those from the two non-thermal processes. Since these are also directly dependent on the external environment, I do not attempt to provide an analytic description of them here.

2.2 Incorporating losses self-consistently in the dynamical model

The implementation of bolometric radiative losses in the original code of Paper 1 was already more sophisticated than the simple calculation described above, because it models the electron energy spectrum of the lobes as a sum of discrete Jaffe & Perola (1973) aged spectra, as described in section 2.3 of Paper 1, and takes account of adiabatic losses while doing so. Thus it models the true time evolution of the term I_E/I_{loss} in the analysis above. It also does not neglect the contribution of the lobe magnetic fields to the energetics. However, it is difficult to modify the dynamical solver of the code, which essentially solves the coupled differential equations for lobe expansion in the longitudinal and transverse directions, to include these realistic losses: for example, the aged spectra depend on the time history of the magnetic field strength which is not readily available inside the numerical solver. Equally, however, the losses cannot just be calculated outside the dynamical solver as was done for Paper 1, because they affect the dynamics through the lobe pressure.

To overcome this problem I implemented an iterative solution. From an existing run of the code, the losses can be calculated, and therefore the total energy in the system taking account of radiative losses,

$$E(t) = \int_0^t (Q - L_{\text{IC}} - L_{\text{synch}} - L_{\text{Brems}}) dt' \quad (14)$$

can be written down, where the three loss terms are respectively due to inverse-Compton, synchrotron and thermal bremsstrahlung from the shocked shell. $E(t)$ is the quantity that affects the dynamics, and which is approximated by Qt in a typical run of the code. Having generated a table of $E(t)$, the code can be run again with the same input parameters but with a linear interpolation of $E(t)$ substituted for Qt in the dynamical and loss calculation parts of the code. (The momentum flux of the jet is unchanged as the radiation processes do not carry away significant net momentum.) This approach converges quite quickly on a solution if $E(t)$ remains positive throughout, but if it does not (i.e. the inverse-Compton emission would remove more energy from the system than it actually contains) then the lookup table for $E(t)$ must be truncated in time, and then more iterations

are necessary for convergence. In these cases the iterative code alternates between solving for the dynamics given the losses for the previous iteration, with no extrapolation, and solving for the losses assuming a continued loss rate after the end of the previous iteration which is equal to the time-weighted average loss rate over the source lifetime. The iterative code can then be run until the typical loss rate converges. In the implementation used for this paper, we require the lifetime of the run not to be increasing and to have converged within 2 per cent, and the relative mean absolute difference between loss rates in the past ten timesteps to be within 10 per cent, in order to decide that the iterations have converged.

3 RESULTS

To see the additional effect of self-consistent losses we need to run the code with and without the iterative loss finding approach described above. The code already accounts for radiative and adiabatic losses in the integrated synchrotron spectrum, and therefore the easiest way to represent the different models is as tracks in the power-linear size (PD) diagram. I ran the code for four redshifts ($z = 0, 2, 4, 6$) and four jet powers ($Q = 10^{37}, 10^{38}, 10^{39}$ and 10^{40} W), modelling evolution over a maximum of 1 Gyr. The highest jet power here is of order the Eddington luminosity for a 10^9 solar mass black hole, and so represents something like the maximum jet power we would expect to observe in the Universe, comparable to that of a powerful source like Cygnus A at $z = 0$, while $Q = 10^{37}$ W is the power observed for the top end of the Fanaroff-Riley class I (FRI) population at $z = 0$; thus these models span the full range of powerful RLAGN. For simplicity all models use the same environment, a universal pressure profile (Arnaud et al. 2010) environment with $M_{500} = 2.5 \times 10^{13} M_{\odot}$, which is not unrealistic for low-redshift radio galaxies; a caveat (which I return to below) is that RLAGN environments are likely to be significantly different at high redshifts, but we keep the environments constant here in order to see the purely redshift-dependent effects of the model.

Results for the luminosity and size of the modelled sources at rest-frame 144 MHz are plotted as a function of redshift in Fig. 1, where I also show the results of the original model without the iterative search for a self-consistent solution and the distribution of AGN at those redshifts from Hardcastle et al. (2025) on the PD diagram. (The Hardcastle et al. (2025) AGN catalogue was based on the optical identification catalogue of Hardcastle et al. (2023), who took all $z > 5$ objects from the work of Gloude-mans et al. (2022) on high-redshift LoTSS quasars, and so these are the objects plotted for the $z = 6$ redshift bin.)

Several features of this figure are of interest. Firstly, we see that, as expected, the self-consistent model gives lower radio luminosity than the Paper 1 model for a given linear size for all redshifts, with the difference increasing with redshift. The offset at $z = 0$ is a result of synchrotron losses at early times, but otherwise at $z = 0$ we see almost no effect of the self-consistent modelling, as the late-time inverse-Compton losses are negligible. At higher redshifts we see an increasing difference between the Paper 1 models and the self-consistent ones with source size/age, corresponding to the increasing importance of inverse-Compton losses with time. Crucially, in the bottom panels of Fig. 1, the tracks in the PD diagram decline steeply once the sources reach physical sizes of 10-100 kpc, as there is no way for them to avoid catastrophic inverse-Compton losses. Relative to the Paper 1 models, there is a large region of parameter space in the PD diagram at large physical sizes that is excluded for sources below a given jet power Q . At high z , sources start their

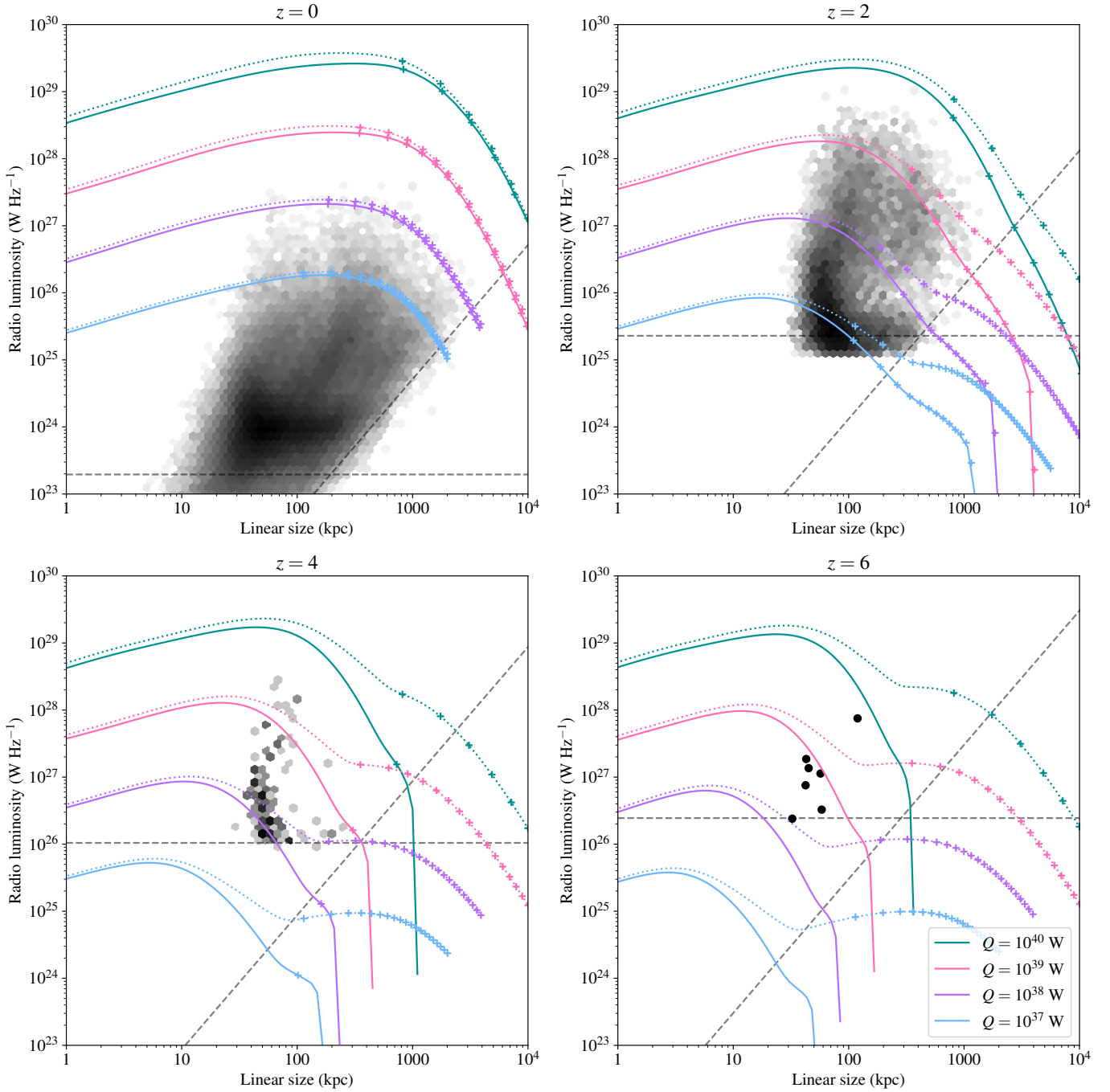


Figure 1. Evolution of radio sources in the power-linear size diagram for different jet powers and redshifts. Radio luminosity is measured at 144 MHz: the rest-frame luminosity at $144(1+z)$ MHz is calculated and then k -corrected back to 144 MHz assuming $\alpha = 0.7$ to mimic the approach used in observations. Panels show the same jet powers and environmental conditions for $z=0$ (top left), $z=2$ (top right), $z=4$ (bottom left) and $z=6$ (bottom right). In all cases four jet powers ($Q = 10^{37}$ W, $Q = 10^{38}$ W, $Q = 10^{39}$ W, $Q = 10^{40}$ W) are represented by coloured lines. Dotted lines represent the evolution in the reference model of Paper 1 and solid lines show the new self-consistent model. Crosses on both sets of lines indicate 50-Myr intervals of the source’s evolution: lines without a cross terminate before the source reaches an age of 50 Myr. Black density plots, or in the case of $z=6$ black individual points, represent the positions of LOFAR RLAGN at these redshifts from [Hardcastle et al. \(2025\)](#), where we include all AGN in that catalogue with redshift within ± 0.5 of the central redshift. As discussed by [Hardcastle et al. \(2023\)](#), the $z \approx 6$ points in this catalogue are all taken from [Gludemans et al. \(2022\)](#). Note that many of the sources on this plot are unresolved, and so their linear sizes as plotted should be taken as upper limits on the true projected linear size. In particular none of the $z \approx 6$ sources is resolved. Grey dashed lines represent the flux limit (horizontal line) and surface brightness limit (diagonal line) of the LOFAR-based [Hardcastle et al. \(2025\)](#) catalogue at the central redshift of the sources plotted.

steep downward trajectory in radio luminosity after only a few tens of Myr in age. The differences between the predicted radio luminosities with and without taking account of self-consistent radiative losses can be as much as two orders of magnitude at the point where the simulated sources intercept the observational surface brightness limit.

Another interesting effect is on the evolution of inverse-Compton emission itself, and this is shown in Fig. 2. The inverse-Compton PD diagram plotted in the Figure is not commonly used observationally because sample sizes of sources with good inverse-Compton measurements are rare, but it can be seen that the model predictions for low-redshift sources are very consistent with observation. However, the predictions for high-redshift sources are very different once the self-consistent losses are included. The maximum achievable inverse-Compton luminosity is greatly reduced at high z and in fact is more or less independent of redshift for a given jet power in the self-consistent models.

Other predictions of the self-consistent models are similar to those of the Paper 1 model. In particular, the evolution of spectral index is very similar, and sources grow to roughly the same size as a function of time, because the longitudinal expansion of the lobes is driven by the jet momentum flux, which is unaffected by radiative losses. The predicted axial ratios of sources in the self-consistent models are systematically smaller at higher redshift, as expected since the losses remove pressure from the lobes and hence reduce the rate at which they expand transversely. This might tend to reduce the feedback effects of these high-redshift sources.

Of course, the use of a single constant environment over the wide range of redshift (and even jet power) modelled here is completely unrealistic, and is intended only to allow the reader to isolate the effects of redshift-dependent losses from all other effects. All other things being equal, we expect typical radio galaxy environments to be poorer (lower M_{500}) in the past, but also to potentially have a lower ratio of hot baryonic mass to dark matter mass and a flatter radial pressure distribution. Lower densities of hot gas tend to make lobes expand faster and so to be less luminous for a given size, but flatter hot gas distributions have the opposite effect (Hardcastle & Krause 2013) and so might push the onset of catastrophic inverse-Compton losses to sources of smaller sizes. All of this, however, really only affects the size-luminosity relationship: the timescale on which inverse-Compton losses start to affect the dynamics is essentially unaffected by environment, by the arguments of Section 2.1.

4 DISCUSSION AND CONCLUSION

In the previous sections I have shown the need for self-consistent modelling of the effects of radiative losses on the dynamical modelling of radio sources from Paper 1, and implemented a simple scheme for making the models self-consistent in the situation where radiative losses are not negligible in terms of the overall energetics of the system. Results are shown in Figs 1 and 2.

Interestingly, the observations shown in Fig. 1 are at least qualitatively consistent with the models described in the previous section. At low redshifts, observed source linear sizes are limited not by RLAGN physics but by the surface brightness limit in the LOFAR observations (which either causes the sources not to be observed at all or to have underestimated sizes) and so the PD diagram has a sharp boundary at its right-hand edge, as seen in the top two panels of Fig. 1. But at high z the observed LOFAR sources are all compact and most populate the area below the $Q = 10^{39}$ W line on the plots – the observational selection effects alone would clearly

(from Fig. 1) allow a population of larger sources to exist, but they do not. Although this could be for other reasons (such as the inadequacy of a single environmental model over all of cosmic time, or a source lifetime distribution at high z which does not allow sources to grow to large sizes), and it is worth noting that the high- z sources are typically quasars and are likely to appear somewhat smaller due to projection, it is a general prediction of the model of this paper that large, luminous sources will be very rare and that the most luminous objects ($\gtrsim 10^{28}$ W Hz $^{-1}$) will only remain in that state for a short period. These effects would of course be even more extreme for redshifts $z > 4$.

These results have implications for the inference of jet powers from radio observations, such as has been carried out using the Paper 1 models by Hardcastle et al. (2019) and Pierce et al. (2026). The effects of self-consistent losses can safely be ignored at low z but by $z \approx 2$ the use of the Paper 1 model (or any other which neglects radiative losses in the source dynamics) would give rise to an underestimate of the jet power which could be quite significant, since it scales close to linearly with the difference in low-frequency luminosity between the two models. This would have the effect of pushing up our estimates of integrated kinetic power as a function of redshift. We will attempt to account for this effect in future analysis.

The results may also have implications for the prospects for studying the 21-cm forest using luminous RLAGN targets to give a direct detection of absorption lines. At the rest-frame GHz frequencies of the required observations, powerful RLAGN at low z are mostly dominated by radio emission from the lobes, which is what is modelled by the semi-analytical models discussed here and in Paper 1. Only a small minority of all RLAGN, aligned close to our line of sight, have observed radio luminosity dominated by the relativistically beamed core and jet. Thus, in considering the population of objects that might provide a bright background for 21-cm studies, it is important to take account of the physics outlined here and in Paper 1 rather than assuming some scaling from the optical properties of quasars (cf., e.g., Niu et al. 2025). Sources with jet powers in the range $10^{39} - 10^{40}$ W, which are required to produce 144-MHz radio flux densities from the lobes of tens of mJy at high redshift, will maintain the required radio luminosity for only a few to a few tens of Myr and so will be substantially rarer than their counterparts at low z , though of course this does not rule out their existence altogether (e.g. Gloudemans et al. 2025).

Finally, the models predict (Fig. 2) that inverse-Compton luminosities of powerful sources essentially have a jet-power-linked maximum at high z , despite the strong increase in the energy density of the CMB. This would affect the conclusions of e.g. Mocz et al. (2011) and make inverse-Compton ‘ghosts’ less prevalent at high redshift, in turn affecting the expectations for observations with next-generation X-ray instruments such as *New-Athena*.

Detailed predictions of the population of RLAGN at these redshifts should take account of the jet generation mechanism, including the distribution of black hole mass, spin and accretion rate, as well as the expected small-scale and large-scale environments which, together with the jet power, determine the source dynamics. Clearly such an effort is beyond the scope of this paper, but forward-modelling of the radio AGN population from cosmological simulations is starting to become realistic: such efforts are complicated by, but very clearly need to take into account, the loss processes that I have discussed above.

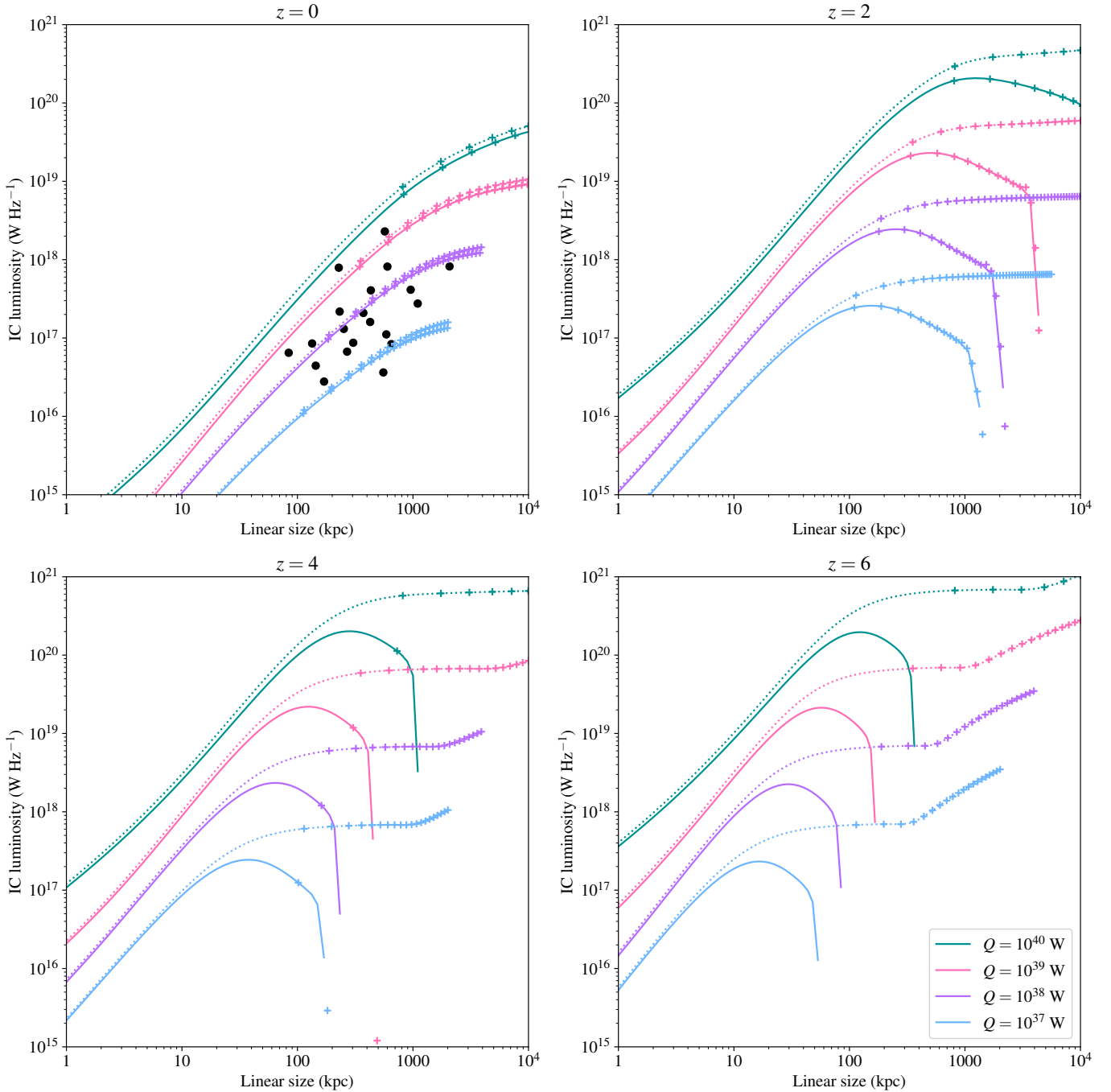


Figure 2. Evolution of radio sources in the inverse-Compton power-linear size diagram for different jet powers and redshifts. As Fig. 1, but here we plot the inverse-Compton luminosity at a rest-frame energy of 1 keV (2.4×10^{17} Hz). Black data points in the $z = 0$ panel are the $z < 0.25$ objects from [Ineson et al. \(2017\)](#).

ACKNOWLEDGMENTS

I acknowledge support from the UK Science and Technology Facilities Council [ST/Y001249/1], and am grateful to Judith Croston and Jonathon Pierce for comments on the manuscript. I also thank the referee, Patrick Yates-Jones, for helpful comments on the submitted version of the paper. This research made use of ASTROPY, a community-developed core Python package for astronomy ([Astropy Collaboration et al. 2013](#)) hosted at <http://www.astropy.org/> and of MATPLOTLIB ([Hunter 2007](#)).

LOFAR is the Low Frequency Array designed and constructed by ASTRON. It has observing, data processing, and data storage facilities in several countries, which are owned by various parties (each with their own funding sources), and which are collectively operated by the LOFAR ERIC under a joint scientific policy. The LOFAR resources have benefited from the following recent major funding sources: CNRS-INSU, Observatoire de Paris and Université d'Orléans, France; BMBF, MIWF-NRW, MPG, Germany; Science Foundation Ireland (SFI), Department of Business, Enterprise

and Innovation (DBEI), Ireland; NWO, The Netherlands; The Science and Technology Facilities Council, UK; Ministry of Science and Higher Education, Poland; The Istituto Nazionale di Astrofisica (INAF), Italy.

This research made use of the Dutch national e-infrastructure with support of the SURF Cooperative (e-infra 180169) and the LOFAR e-infra group. The Jülich LOFAR Long Term Archive and the German LOFAR network are both coordinated and operated by the Jülich Supercomputing Centre (JSC), and computing resources on the supercomputer JUWELS at JSC were provided by the Gauss Centre for Supercomputing e.V. (grant CHTB00) through the John von Neumann Institute for Computing (NIC).

This research made use of the University of Hertfordshire high-performance computing facility and the LOFAR-UK computing facility located at the University of Hertfordshire and supported by STFC [ST/P000096/1], and of the Italian LOFAR IT computing infrastructure supported and operated by INAF, and by the Physics Department of Turin university (under an agreement with Consorzio Interuniversitario per la Fisica Spaziale) at the C3S Supercomputing Centre, Italy.

DATA AVAILABILITY

No data were newly processed for this paper. Catalogued data for the LOFAR AGN sample used in the plots is available at https://lofar-surveys.org/dr2_release.html.

REFERENCES

- Arnaud M., Pratt G. W., Piffaretti R., Böhringer H., Croston J. H., Pointecouteau E., 2010, *A&A*, 517, A92
- Astropy Collaboration et al., 2013, *A&A*, 558, A33
- Blandford R. D., Znajek R. L., 1977, *MNRAS*, 179, 433
- Fanaroff B. L., Riley J. M., 1974, *MNRAS*, 167, 31P
- Gludemans A. J., et al., 2022, *A&A*, 668, A27
- Gludemans A. J., et al., 2025, *ApJ*, 980, L8
- Hardcastle M. J., 2018, *MNRAS*, 475, 2768
- Hardcastle M. J., Krause M. G. H., 2013, *MNRAS*, 430, 174
- Hardcastle M. J., et al., 2019, *A&A*, 622, A12
- Hardcastle M. J., et al., 2023, *A&A*, 678, A151
- Hardcastle M. J., et al., 2025, *MNRAS*, 539, 1856
- Hunter J. D., 2007, *Computing In Science & Engineering*, 9, 90
- Ineson J., Croston J. H., Hardcastle M. J., Mingo B., 2017, *MNRAS*, 467, 1586
- Jaffe W. J., Perola G. C., 1973, *A&A*, 26, 423
- Koopmans L., et al., 2015, in *Advancing Astrophysics with the Square Kilometre Array (AASKA14)*. p. 1 ([arXiv:1505.07568](https://arxiv.org/abs/1505.07568)), doi:10.22323/1.215.0001
- Longair M. S., 2010, *High Energy Astrophysics*. Cambridge University Press, Cambridge
- Maiolino R., et al., 2024, *A&A*, 691, A145
- Mellema G., et al., 2013, *Experimental Astronomy*, 36, 235
- Mocz P., Fabian A. C., Blundell K. M., 2011, *MNRAS*, 413, 1107
- Niu Q., Li Y., Xu Y., Guo H., Zhang X., 2025, *ApJ*, 978, 145
- Pierce J. C. S., Sweijen F., Hardcastle M. J., Morabito L. K., Röttgering H. J. A., Baldi R. D., 2026, *MNRAS* in press
- Wu J., Ghisellini G., Hodges-Kluck E., Gallo E., Ciardi B., Haardt F., Sbarato T., Tavecchio F., 2017, *MNRAS*, 468, 109